Hindawi
Advances in Astronomy
Volume 2022, Article ID 8100523, 17 pages
https://doi.org/10.1155/2022/8100523

Research Article

The Restricted Six-Body Problem with Stable Equilibrium Points and a Rhomboidal Configuration

M. A. R. Siddique and A. R. Kashif

Department of Mathematics, Capital University of Science and Technology, Zone-V, Islamabad, Pakistan

Correspondence should be addressed to M. A. R. Siddique; atique.pathan@hotmail.com

Received 1 February 2022; Revised 24 April 2022; Accepted 6 June 2022; Published 17 August 2022

Academic Editor: Zdzislaw E. Musielak

We explore the central configuration of the rhomboidal restricted six-body problem in Newtonian gravity, which has four primaries m_i (where $i = 1, \ldots 4$) at the vertices of the rhombus $(a, 0)$, $(-a, 0)$, $(0, b)$, and $(0, -b)$, respectively, and a fifth mass m_0 is at the point of intersection of the diagonals of the rhombus, which is placed at the center of the coordinate system (i.e., at the origin $(0, 0)$). The primaries at the rhombus's opposite vertices are assumed to be equal, that is, $m_1 = m_2 = m$ and $m_3 = m_4 = \tilde{m}$. After writing equations of motion, we express m_0, m, and $\tilde{m}$ in terms of mass parameters a and b. Finally, we find the bounds on a and b for positive masses. In the second part of this article, we investigate the motion and different features of a test particle (sixth body m_5) with infinitesimal mass that moves under the gravitational effect of the five primaries in the rhomboidal configuration. All four cases have 16, 12, 20, and 12 equilibrium points, with case-I, case-II, and case-III having stable equilibrium points. A significant shift in the position and the number of equilibrium points was found in four cases with the variations of mass parameters a and b. The regions for the possible motion of test particles have been discovered. It has also been observed that as the Jacobian constant C increases, the permissible region of motion expands. We also have numerically verified the linear stability analysis for different cases, which shows the presence of stable equilibrium points.

1. Introduction

The system of point masses is considered to be under motion due to the mutual gravitational force as explained by Newton's gravitational law. Dynamical systems with n point masses have been extensively studied, and various models have been proposed for research aiming at approximating the behaviour of real celestial systems. There are many reasons for studying the n-body problem since it is known that approximately two-thirds of the stars in our Galaxy exist as part of multistellar systems.

In celestial mechanics, the central configuration (CC) plays an important role in the investigation of n-body problems. It is the configuration that can be used to find simple or special solutions of the n-body problem since the shape of the figure formed by the arrangement of the bodies remains constant for all time. That is why the CCs lead to homographic solutions. The first three collinear homographic solutions for $n = 3$ were found by Euler in 1767, and two equilateral triangular homographic solutions were found by Lagrange [1] in 1772 for $n = 3$. The central configuration for $n > 3$ has been investigated a lot. Xia [2] used the analytical continuation approach to find the exact number of CCs for an open set of n positive masses in 1991. Llibre and Mello [3] investigated 7-body problem for the existence of families of central configurations. In 2017, Deng et al. [4] investigated the central configuration of four-body problem with equal masses and showed that for the planar Newtonian four-body problem having adjacent equal masses, that is, $m_1 = m_2 \neq m_3 = m_4$, and equal lengths for the two diagonals, any convex noncollinear central configuration must have a symmetry and must be an isosceles trapezoid. They also showed that when the length between m_1 and m_4 equals the length between m_2 and m_3, the central configuration is also an isosceles trapezoid. In the same year, Marchesin [5] explored the stability of rhomboidal

configurations with a mass in the center. He considered a system with five bodies at $r_0 = (0, 0)$, $r_1 = (a, 0)$, $r_2 = (-a, 0)$, $r_3 = (0, b)$, and $r_4 = (0, -b)$ with masses m_0, $m_1 = m_2 = m$ and $m_3 = m_4 = \tilde{m}$ that are moving in a plane. They investigated the effect of altering the mass of the central body on the stability of such a configuration for several values of mass parameter $\lambda = m/\tilde{m}$. Saari [6] studied the role and properties of central configuration for n-body problem, and the other work on central configuration is given in Refs. [7–15] (for latest publications on CCs, cf. Suraj et al. [16], Zotos, and Papadakis [17], and Cornelio et al. [18]).The three-body problem has been a great challenge for the scientists as it needed some special assumptions for the third body. The ever first problem solved using restriction for the infinitesimal body is "restricted three-body problem" (RTBP). The RTBP originally arose from the work of Newton, but unfortunately, Newton was unable to solve the problem throughout his life. Alexis Clairaut [19, 20] in 1747 solved the problem with some approximations, and in 1757, he calculated the return of "Halley's Comet." Ollongren [21] in 1988 was the first to introduce the restricted five-body problem. Ollongren investigated the motion of the fifth infinitesimal mass that moved under the gravitational attraction of the other four massive bodies. He discovered nine equilibrium points, three of which were stable, and the rest were linearly unstable. In 2007, Papadakis and Kavanos [22] extended the work of Ollongren and investigated the restricted five-body problem numerically, and they showed that the counts of equilibrium points depend on the radiation factors as well as on the mass parameter. Marchesin and Vidal [23] in 2013 studied the stability of five-body problem by assuming that the central body makes a generalized force on the other four bodies. In 2018, Aggarwal et al. [24] investigated the effect of small perturbation in Coriolis and centrifugal forces on the presence of equilibrium points in the restricted four-body problem. The three primaries were placed at the vertices of equilateral triangle and the fourth infinitesimal mass moves under the gravitational effect of the primaries. They showed the existence of 8 to 10 equilibrium points and found that all the liberation points are unstable. Mello et al. [25], in 2009, introduced the stacked CC for the spatial six-body problem, and they illustrated three novel families of stacked spatial central configurations for the six-body problem with a regular tetrahedron model. Recently, in 2020, Idrisi and Ullah [26] investigated the existence and linear stability of equilibrium points in a six-body problem with a square CC and a central mass, and discovered that there are twelve equilibrium points, four of which are stable for a given value of the mass parameter μ_c. Furthermore, in 2020 [27], Ansari et al. studied six body CC by placing the primary at the vertices of a square and a fifth mass at the center of a circle, which is thought to be the orbit of motion for the rest of the primaries. Using the Jeans law and the Mesheherskii space time transformation, they discovered twelve equilibrium points for the sixth small body of variable mass, all of which are unstable. Kulesza et al. [28] in the restricted rhomboidal five-body problem found that the number of libration points depends on the semidiagonal ratio λ and they showed that there can be eleven, thirteen, and even fifteen libration points. In 2013, Marchesin and Vidal [29] studied the restricted rhomboidal five-body problem and found that no chaos exists and the behaviour of the fifth mass is quite predictable. They also showed the existence of the periodic solutions of infinitesimal mass and also studied numerically their linear horizontal stability. The rhomboidal six-body CC was presented by Siddique et al. in 2021 [30] by putting the four primaries at the corners of the rhombus and the fifth mass at the intersection of the two diagonals of rhombus. They computed the region of probable motion of the sixth mass using the first integral of motion and the values of the Jacobian constant C for various energy intervals and found the limitation on the region of motion for infinitesimal mass. They demonstrated the existence and uniqueness of equilibrium solutions on and off the axes using semi-analytic approaches, and established that there are always twelve unstable equilibrium points when $b \in (1/\sqrt{3}, 1.1394282249562009)$ and $a = 1$. Recently, Ref. [31] examined the basins of convergence by deploying the well-known Newton–Raphson iterative scheme, associated with the libration points (indeed, act as attractors), in the restricted rhomboidal six-body problem.

In this study, we focus on the rhomboidal restricted six-body problem, which has four primaries at the corners of the rhombus and a fifth primary where the diagonals of the rhombus cross, which is in the center of the coordinate system, that is, $(0, 0)$. There is a sixth test mass m_5 that moves under the gravitational effect of the five primaries. The primaries at the opposite vertices of rhombus are assumed to be equal, that is, $m_1 = m_2 = m$ and $m_3 = m_4 = \tilde{m}$. In section 2, we investigate the continuous families of five primaries central configurations for different values of the mass parameters a and b. In section 3, we derived the equation of motion for infinitesimal mass and discovered the Jacobian constant C. In section 4, we explore the Hill's and permissible regions of motion of the m_5. Sections 5 and 6 analyze the positions and stability of the equilibrium points for the sixth body, m_5. Concluding remarks are given in section 7.

2. Rhomboidal Central Configurations

The classical equation of motion for the n-body problem has the following form:

$$m_i \ddot{r}_i = \sum_{j=0, j\neq i}^{n} m_i m_j \frac{\left(\mathbf{r}_j - \mathbf{r}_i\right)}{\left|\mathbf{r}_j - \mathbf{r}_i\right|^3}, \tag{1}$$

where the units are chosen so that the gravitational constant is equal to one. A central configuration is a particular configuration of the n-bodies where the acceleration vector of each body is proportional to its position vector, and the constant of proportionality is the same for the n-bodies. Therefore, a central configuration is a configuration that satisfies the following equation:

$$-\omega^2\left(\mathbf{r}_i-\mathbf{c}\right)=\sum_{j=0,j\neq i}^{n} m_i m_j \frac{\left(\mathbf{r}_j-\mathbf{r}_i\right)}{\left|\mathbf{r}_j-\mathbf{r}_i\right|^3}, \tag{2}$$

where ω is an angular speed and

$$\mathbf{c}=\frac{\sum_{i=1}^{n} m_i\mathbf{r}_i}{\sum_{i=1}^{n} m_i}, \tag{3}$$

is the center of mass on n-bodies. We choose the coordinates (for positions, see Figure 1) of five primaries m_j, where $j = 0-4$ as

$$\mathbf{r}_0=0,\ \mathbf{r}_1=ae^{i\omega t},\ \mathbf{r}_2=-ae^{i\omega t},\ \mathbf{r}_3=bie^{i\omega t},\ \mathbf{r}_4=-bie^{i\omega t}. \tag{4}$$

Expanding equation (2) for $(i=0-4)$ and using equation (3) and letting $m_1=m_2=m$ and $m_3=m_4=\tilde{m}$, we get the following equation for central configurations for the masses m_1 and m_2:

$$\omega^2=\frac{m_0}{a^3}+\frac{2\tilde{m}}{\left(a^2+b^2\right)^{3/2}}+\frac{m}{4a^3}, \tag{5}$$

and for the masses m_3 and m_4, the equation of motion is

$$\omega^2=\frac{m_0}{b^3}+\frac{2m}{\left(a^2+b^2\right)^{3/2}}+\frac{\tilde{m}}{4b^3}. \tag{6}$$

The mass m_0 is stationery so its equation of motion ends up zero. We take sum of all primaries is equal to unity that is

$$m_0+2\left(m+\tilde{m}\right)=1. \tag{7}$$

Taking $\omega=1$ and solving equations (5)–(7) give

$$m(a,b)=\frac{N_m}{D(a,b)}, \tag{8}$$

$$\tilde{m}(a,b)=\frac{N_{\tilde{m}}}{D(a,b)}, \tag{9}$$

$$D(a,b)=P_1-P_2, \tag{10}$$

where

$$\begin{aligned}
N_m&=A(a,b)\left(1+7a^3-8b^3\right)-(1-b),\\
N_{\tilde{m}}&=B(a,b)\left(1-8a^3+7b^3\right)-(1-a),\\
A(a,b)&=\frac{\left(a^2+b^2\right)^{3/2}}{8a^3\left(1+b+b^2\right)},\\
B(a,b)&=\frac{\left(a^2+b^2\right)^{3/2}}{8b^3\left(1+a+a^2\right)},\\
P_1&=15a^6+45a^4b^2+64a^3b^3+45a^2b^4+15b^6,\\
P_2&=64\sqrt{a^2+b^2}\left(a^5+a^3b^2+a^2b^3+b^5\right).
\end{aligned} \tag{11}$$

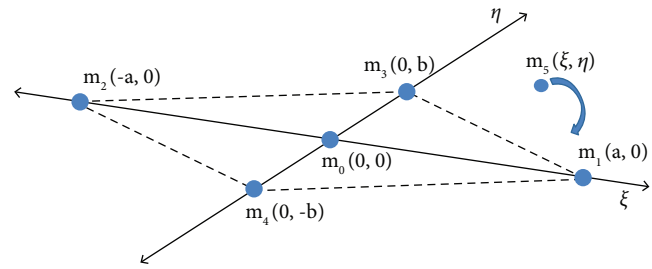

Figure 1: The restricted six-body problem.

Lemma 1. *For any $a>0$ and $b>0$, $D(a,b)$ is always negative.*

Proof. Let us define the following:

$$P(\alpha)=\frac{P_1(\alpha)}{P_2(\alpha)}=\frac{15+45\alpha^2+64\alpha^3+45\alpha^4+15\alpha^6}{64\sqrt{1+\alpha^2}\left(1+\alpha^2+\alpha^3+\alpha^5\right)},\quad \alpha=\frac{b}{a},$$

$$\frac{dP(\alpha)}{d\alpha}=\frac{2(\alpha-1)\left(15\alpha^6+64\alpha^5+109\alpha^4+64\alpha^3+109\alpha^2+64\alpha+15\right)}{64\left(\alpha^2+1\right)^{5/2}\left(\alpha^3+1\right)^2}. \tag{12}$$

To prove $D(a,b)<0$, we need to prove $P(\alpha)<1$. For this, differentiate $P(\alpha)$ with respect to α and find the critical points of $P(\alpha)$ in $(0,\infty)$. There is only one critical point of $P(\alpha)$ (i.e., $\alpha=1$) in $(0,\infty)$ and $P(1)=(23/32\sqrt{2})$. One can easily see that $P(\alpha)$ is monotonically increasing function because $(dP(\alpha)/d\alpha)<0$ in $(0,1)$ and $P(\alpha)$ is monotonically decreasing function because $(dP(\alpha)/d\alpha)>0$ in $(1,\infty)$ (see Figure 2). When $\alpha\longrightarrow 0$ or ∞, $P(\alpha)\longrightarrow(15/64)$. So $P(\alpha)<1$ for $\alpha\in(0,\infty)$, and hence, $D(a,b)<0$ for $a>0$ and $b>0$.

To prove $m(a,b)$ and $\tilde{m}(a,b)$ positive, we need to prove N_m and $N_{\tilde{m}}$ must be negative for $a>0$ and $b>0$. Because N_m and $N_{\tilde{m}}$ are nonlinear algebraic functions of a and b, so it is difficult to solve these inequalities. For this, we draw the region (shaded region of Figure 3) where both N_m and $N_{\tilde{m}}$ are negative. From the graph, we can easily find the approximate bounds for $a>0$ and $b>0$ where N_m and $N_{\tilde{m}}$ are negative.

Using equation (7) to equation (9), one can easily see that $m(a,b)=\tilde{m}(b,a)$ and $0<m(a,b)<0.5$, $0<\tilde{m}(a,b)<0.5$ and $m_0(a,b)>0$ for $0.5<a<1$ and $0.5<b<1$. In Figure4 we show the region of central configuration for which $m,\tilde{m},m_0>0$ are positive. Because Figure 4 is symmetric about the line $b=a$, we divide here Figure 4 into two parts: upper region (R_u) and lower region (L_u). Here, we discuss only the central configuration for the region of R_u. The upper CC region is approximately surrounded by the following three interpolating polynomials:

$$\begin{aligned}
f_1&=a,\\
f_2&=-220.187a^7+1310.43a^6-3257.57a^5+4399.05a^4\\
&\quad-3494.37a^3+1637.89a^2-421.05a+46.8139,\\
f_3&=259.785a^6-1127.86a^5+2021.17a^4\\
&\quad-1914.65a^3+1013.31a^2-284.941a+34.1992.
\end{aligned} \tag{13}$$

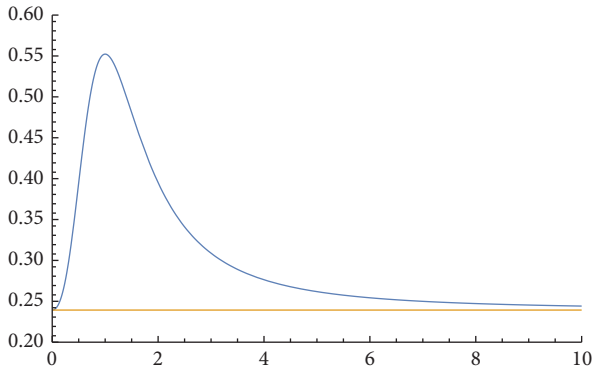

Figure 2: Graph of $P(\alpha)$.

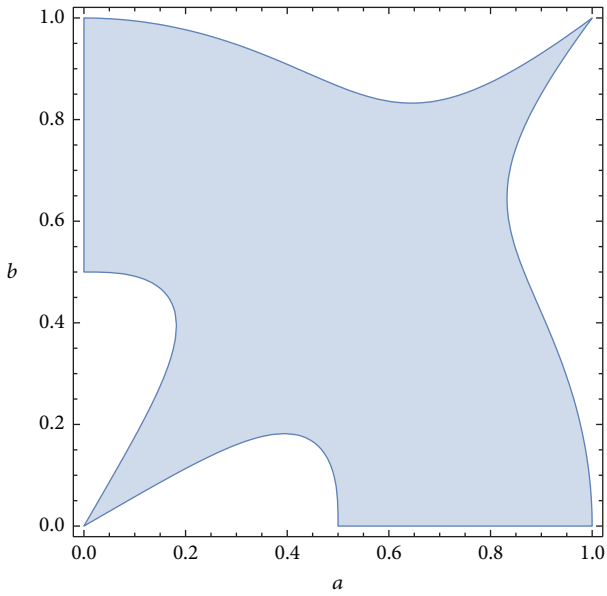

Figure 3: N_m and $N_{\tilde{m}}$ both are negative (shaded region).

Figure 5 shows the changes of masses m_0, m, and $\tilde{m}$ with variations of parameter b. We can clearly see that as b varies in $(0.5, 1)$, the mass m_0 is increasing, and other masses are becoming zeros. □

3. Equation of Motion of Infinitesimal Body

In this section, we derive the equation of motion of the infinitesimal body, m_5, that moves under the gravitational attraction of the five primaries. The sixth body has a significantly smaller mass as compared to the masses of the primaries, that is, $(m_5 \ll m_i)$ where $i = 0 - 4$. Due to this fact, the sixth body acts as an infinitesimal test particle, and therefore, it does not have any influence on the motion of the five primaries. In the above scenario, the equation of motion of the test particle m_5 is

$$\ddot{r}_5 = -\sum_{i=0}^{4} m_i \frac{\mathbf{r}_5 - \mathbf{r}_i}{\left|\mathbf{r}_5 - \mathbf{r}_i\right|}. \tag{14}$$

The dot represents the derivative with reference to time. We discuss here the dynamics of the infinitesimal mass with respect to the five primaries. The equations of motion of the m_5 in synodical coordinates ξ and η [32] are

$$\begin{aligned} \ddot{\xi} - 2\dot{\eta} &= \Omega_\xi, \\ \ddot{\eta} + 2\dot{\xi} &= \Omega_\eta, \end{aligned} \tag{15}$$

where

$$\Omega(\xi, \eta) = \frac{\left(\eta^2 + \xi^2\right)}{2} + \frac{m_0}{r_{50}} + m\left(\frac{1}{r_{51}} + \frac{1}{r_{52}}\right) + \tilde{m}\left(\frac{1}{r_{53}} + \frac{1}{r_{54}}\right), \tag{16}$$

is the effective potential, where the mutual distances are

$$\begin{aligned} r_{50} &= \sqrt{\xi^2 + \eta^2}, \\ r_{51} &= \sqrt{(\xi - a)^2 + \eta^2}, \\ r_{52} &= \sqrt{(\xi + a)^2 + \eta^2}, \\ r_{53} &= \sqrt{\xi^2 + (\eta - b)^2}, \\ r_{54} &= \sqrt{\xi^2 + (\eta + b)^2}. \end{aligned} \tag{17}$$

The effective potential is shown in Figure 6 (right) for the four different cases of rhomboidal restricted six-body problem. We define the first Jacobian-type integral by

$$C = \frac{1}{2}\left(\dot{\xi}^2 + \dot{\eta}^2\right) - \Omega. \tag{18}$$

By demonstrating that $\dot{C}(\xi, \eta) = 0$, it is now straightforward to establish that $C(\xi, \eta)$ is the first integral of motion of system (18).

Equation (18) shows that $C + \Omega \geq 0$. Then, $\Omega = -C$ will establish a boundary between both the allowed and forbidden regions and $\Omega = -C$ presents the zero velocity curves for various values of C.

4. The Spheres of Influence

Spheres of influence or gravitational spheres of influence are areas surrounding celestial objects where other celestial objects experience the greatest pull and can become satellites of the huge celestial object relative to its mass; these regions are also known as Hill's regions, after *George William Hill*. The zero velocity curves (ZVC) are the contours of the Jacobian constant C as mentioned above, and they are available in Figure 6 on the left, with their corresponding effective potentials on the right. The Hill's regions are tightly packed circular regions surrounding primaries; in Figure 6 (i), for case-I when $b = 0.58$ and $a = 0.68$, the Hill's region for m_1 stretches between L_2 and L_4, whereas for m_3, it extends between L_5 and L_7. Figure 6 (i) also shows that the spheres of influence shrink as the particle mass decreases, since m_0 has a relatively tiny Hill's region as compared to the other primaries. The pink and green lines in Figures 6 (i), (iii), (v), and (vii) on the left depict the contours of equations (19) and (20). The black dots indicate masses and are represented by the symbol m_i; $i = 0, 1, 2, 3, 4$, the orange dots

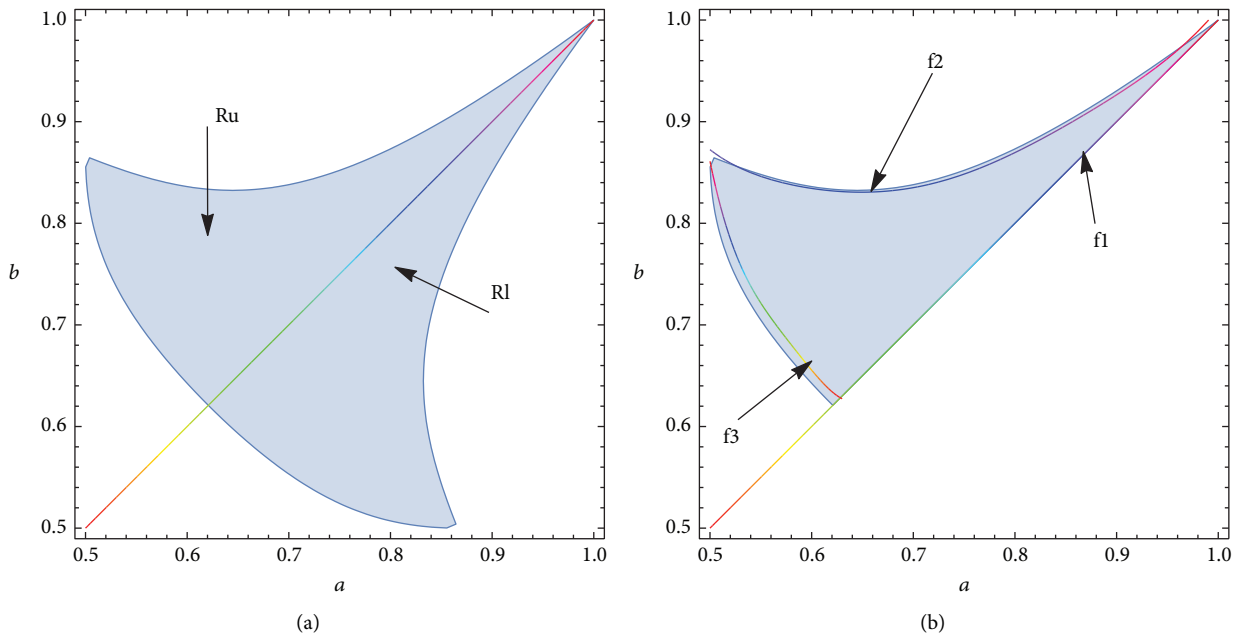

FIGURE 4: (a) Central configuration region (shaded): (b) upper central configuration is surrounded by three interpolating curves (hue color).

represent equilibrium points and are denoted by L_i; $i = 1, 2, \ldots, 20$. Figures 6 (ii), (iv), (vi), and (viii) on right illustrate the effective potentials for each of the four cases, where the closely packed circular regions around the potentials of each mass, which resemble chimneys, can be seen clearly. The permissible regions of motion for the infinitesimal mass m_5 are shown in Figures 7–10 for each of the four cases for different values of mass parameters a and b. Six figures for each of the four cases show the forbidden (shaded) and permissible (white) regions of motion of m_5 for various values of C. The regions of motion that are permitted have the same behaviour in all four cases; that is, the permissible region increases as the value of C decreases. It has also been numerically confirmed that the permissible regions of motion are connected and are around the primaries for higher values of C, that is, at $C = -1.66, -1.97, -2.47, -2.59$, and -3.49. The permissible motion regions are mainly around the four primary and are isolated from one another at $C = -1.78$, and for the above values of C, the motion of m_5 will be bounded around any of the four primaries and will not be able to escape form there normally. The permitted regions become totally detached when $C \leq -1.58$, and the infinitesimal mass m_5 may freely move in the gravitational field of the primaries.

5. Equilibrium Solutions

All rates of change should be zero for equilibrium solutions; hence, the right-hand side of the system in (15) can be set to zero, that is, $\Omega_\xi = 0$ and $\Omega_\eta = 0$, and the solution of resulting equations will give the problem's equilibrium solutions. Ω_ξ and Ω_η are

$$\Omega_\xi = \xi - \frac{m_0\xi}{\left(\eta^2+\xi^2\right)^{3/2}} - m\left(\frac{\xi-a}{\left((\xi-a)^2+\eta^2\right)^{3/2}} + \frac{a+\xi}{\left((a+\xi)^2+\eta^2\right)^{3/2}}\right) - \tilde{m}\left(\frac{\xi}{\left((\eta-b)^2+\xi^2\right)^{3/2}} + \frac{\xi}{\left((b+\eta)^2+\xi^2\right)^{3/2}}\right), \tag{19}$$

$$\Omega_\eta = \eta - \frac{m_0\eta}{\left(\eta^2+\xi^2\right)^{3/2}} - m\left(\frac{\eta}{\left((\xi-a)^2+\eta^2\right)^{3/2}} + \frac{\eta}{\left((a+\xi)^2+\eta^2\right)^{3/2}}\right) - \tilde{m}\left(\frac{\eta-b}{\left((\eta-b)^2+\xi^2\right)^{3/2}} + \frac{b+\eta}{\left((b+\eta)^2+\xi^2\right)^{3/2}}\right). \tag{20}$$

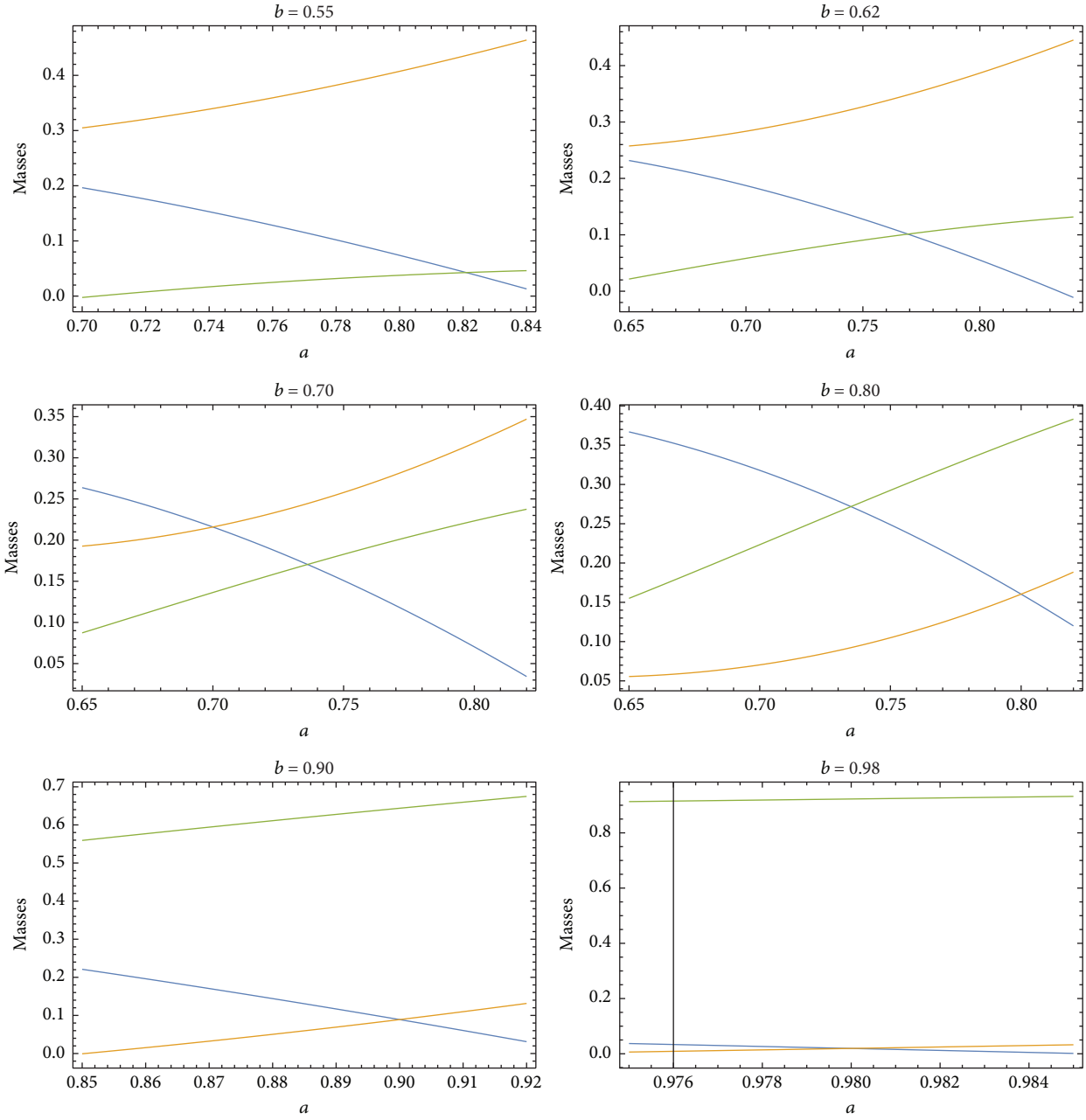

Figure 5: Variations of primary masses m_0 (green), $\tilde{m}$ (orange), and m (blue) for different values of b.

We considered four cases with different values of a and b that show a significant change in the number and location of equilibrium points, namely, $a = 0.68$ and $b = 0.58$ for case-I; $a = 0.68$ and $b = 0.60$ for case-II, $a = 0.78$ and $b = 0.67$ for case-III; and $a = 0.62$ and $b = 0.80$ for case-IV. The corresponding equilibrium points can be seen in subfigures (i), (iii), (v), and (vii) of Figure 6.

5.1. Equilibrium Solutions: On the Coordinate Axes. We shall limit our investigation to the first quadrant, $\xi \geq 0$ and $\eta \geq 0$, because the potential given in equation (15) is unchanged under the symmetry $(\xi, -\eta)$, $(-\xi, \eta)$, and $(-\xi, -\eta)$. To determine the presence and number of equilibrium solutions on the y-axis, we set $\xi = 0$ and then write equations (19) and (20) as

$$\begin{aligned} \Omega_\xi &= 0, \\ \Omega_\eta &= \eta - \frac{m_0\eta}{\left(\eta^2\right)^{3/2}} - \frac{2m\eta}{\left(a^2+\eta^2\right)^{3/2}} \\ &\quad - \tilde{m}\left(\frac{\eta - b}{\left((\eta - b)^2\right)^{3/2}} + \frac{b+\eta}{\left((b+\eta)^2\right)^{3/2}}\right). \end{aligned} \tag{21}$$

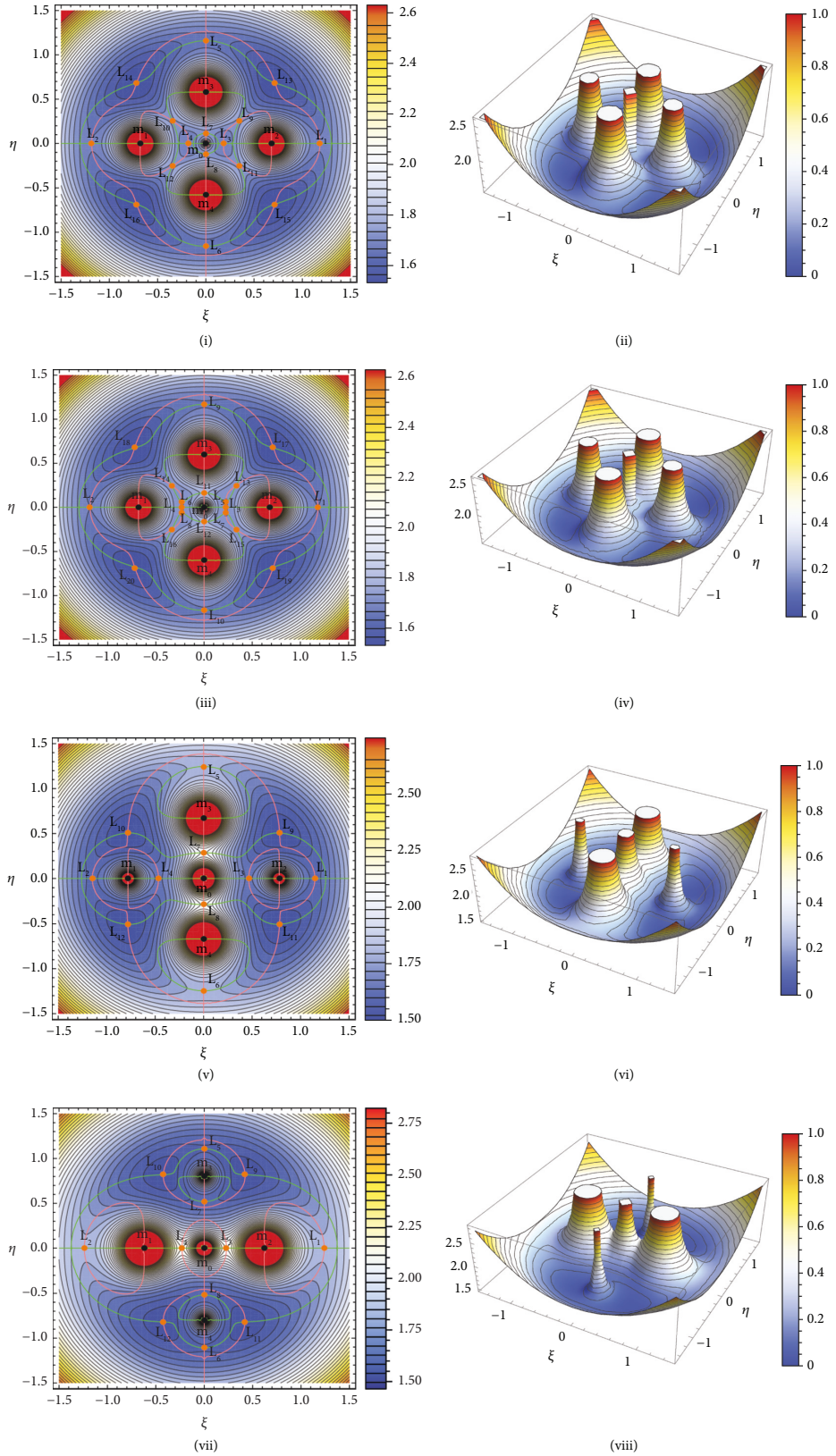

FIGURE 6: Left: zero velocity curves and contour plots with Lagrange points for different values of a and b in 2D, Right: corresponding effective potential for different values of a and b, $a = 0.68$ and $b = 0.58$: for (i) and (ii), $a = 0.68$ and $b = 0.60$: for (iii) and (iv), $a = 0.78$ and $b = 0.67$: for (v) and (vi), $a = 0.62$ and $b = 0.80$: for (vii) and (viii).

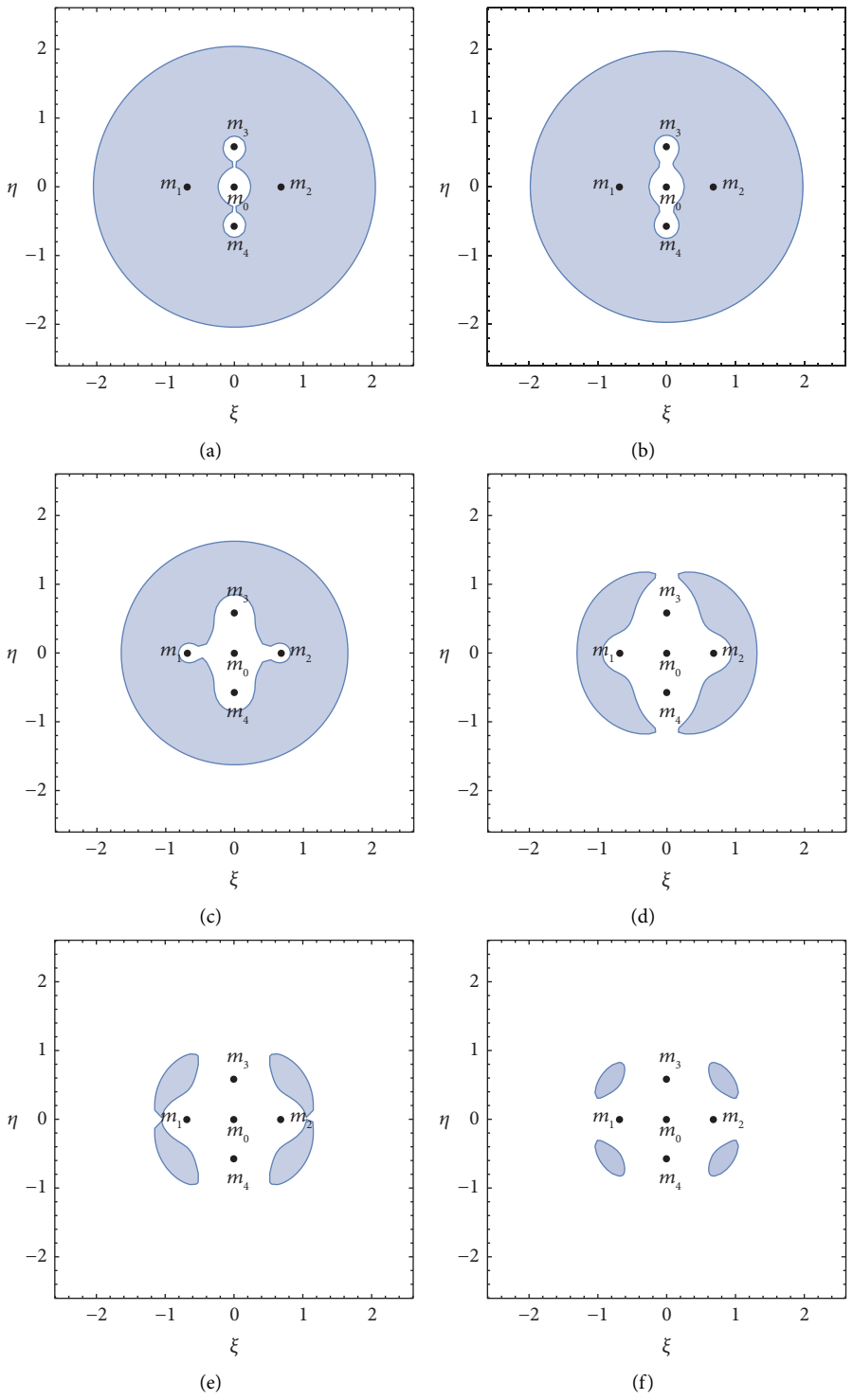

Figure 7: The permitted (white) and prohibited (shaded) regions of motion of m_5 for the $C \in (-2.59, -1.54)$ when $b = 0.58$ and $a = 0.68$: (a) $C = -2.59$, (b) $C = -2.47$, (c) $C = -1.97$, (d) $C = -1.64$, (e) $C = -1.57$, and (f) $C = -1.54$.

The η axis is subdivided into $0 < \eta < b$ and $\eta > b$ to figure out $\Omega_\eta = 0$ for equilibrium solutions. $\eta = b$ means collisions of m_5 with m_3 or m_4 from inside. We will not discuss collisions cases here.

5.2. $0 < \eta < b$. Equation (21) is rewritten as

$$f_1(\eta) = \eta - \frac{m_0}{\eta^2} - \frac{2m\eta}{\left(a^2 + \eta^2\right)^{3/2}} - \tilde{m}\left(\frac{1}{(\eta - b)^2} + \frac{1}{(b + \eta)^2}\right). \quad (22)$$

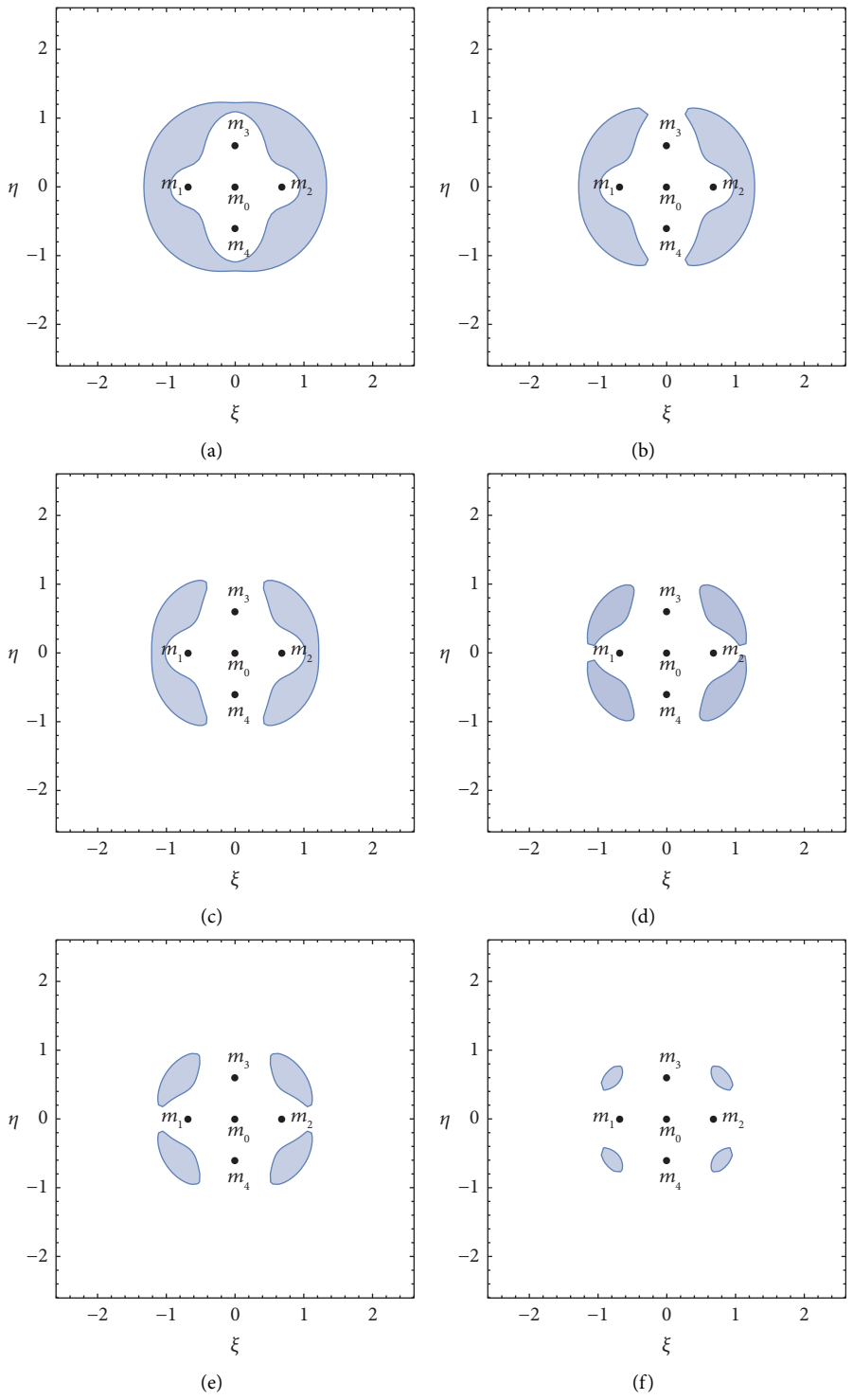

FIGURE 8: The permitted (white) and prohibited (shaded) regions of motion of m_5 for the $C \in (-1.66, -1.53)$ when $b = 0.60$ and $a = 0.68$: (a) $C = -1.66$, (b) $C = -1.63$, (c) $C = -1.60$, (d) $C = -1.58$, (e) $C = -1.57$, and (f) $C = -1.53$.

For $\eta \in (0, b)$ and $b \in (0.5, 1)$, when $\eta \approx 0$, $f_1(\eta) < 0$ and when $\eta \approx b$, $f_1(\eta) > 0$; thus, the mean value theorem implies that $f_1(\eta)$ has at least one zero when $\eta \in (0, b)$. To verify the existence and uniqueness of equilibrium solutions inside the interval $(0, b)$, we take derivative of equation (22):

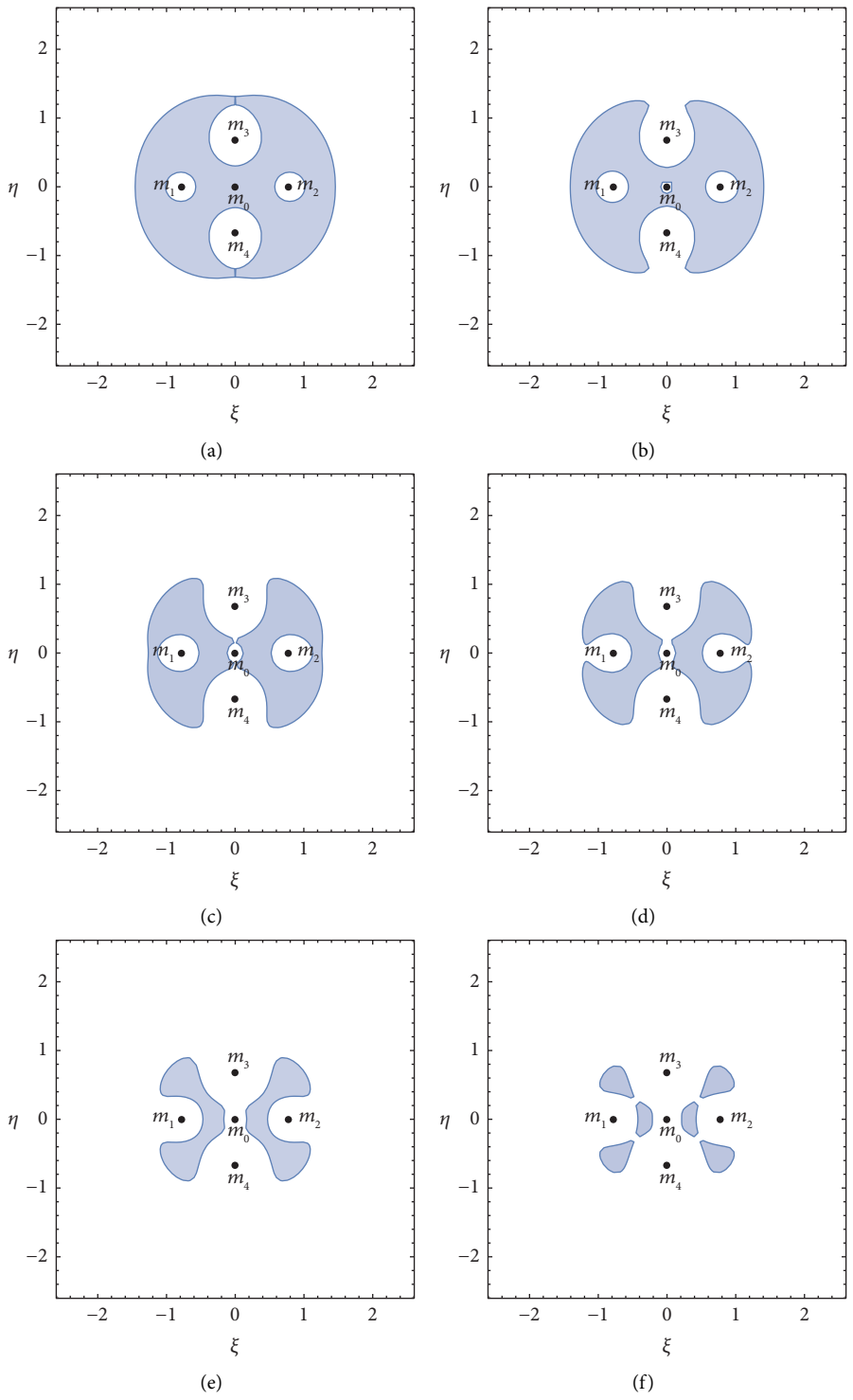

Figure 9: The permitted (white) and prohibited (shaded) regions of motion of m_5 for the $C \in (-1.78, -1.54)$ when $b = 0.67$ and $a = -0.78$: (a) $C = -1.78$, (b) $C = -1.74$, (c) $C = -1.66$, (d) $C = -1.64$, (e) $C = -1.58$, and (f) $C = -1.54$.

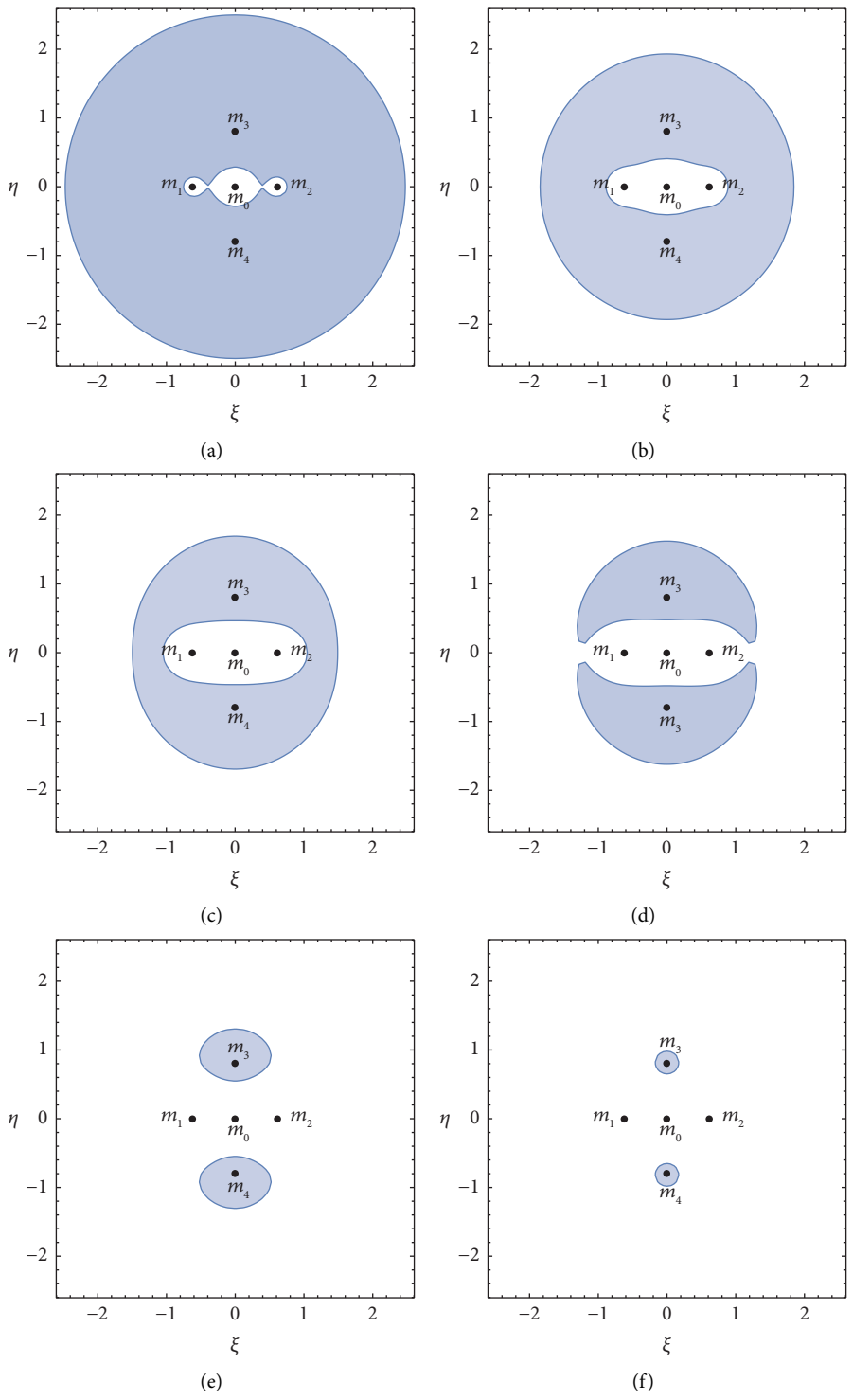

FIGURE 10: The permitted (white) and prohibited (shaded) regions of motion of m_5 for the $C \in (-3.49, -0.30)$ when $b = 0.80$ and $a = 0.62$: (a) $C = -3.49$, (b) $C = -2.31$, (c) $C = -1.91$, (d) $C = -1.80$, (e) $C = -1.32$, and (f) $C = -0.30$.

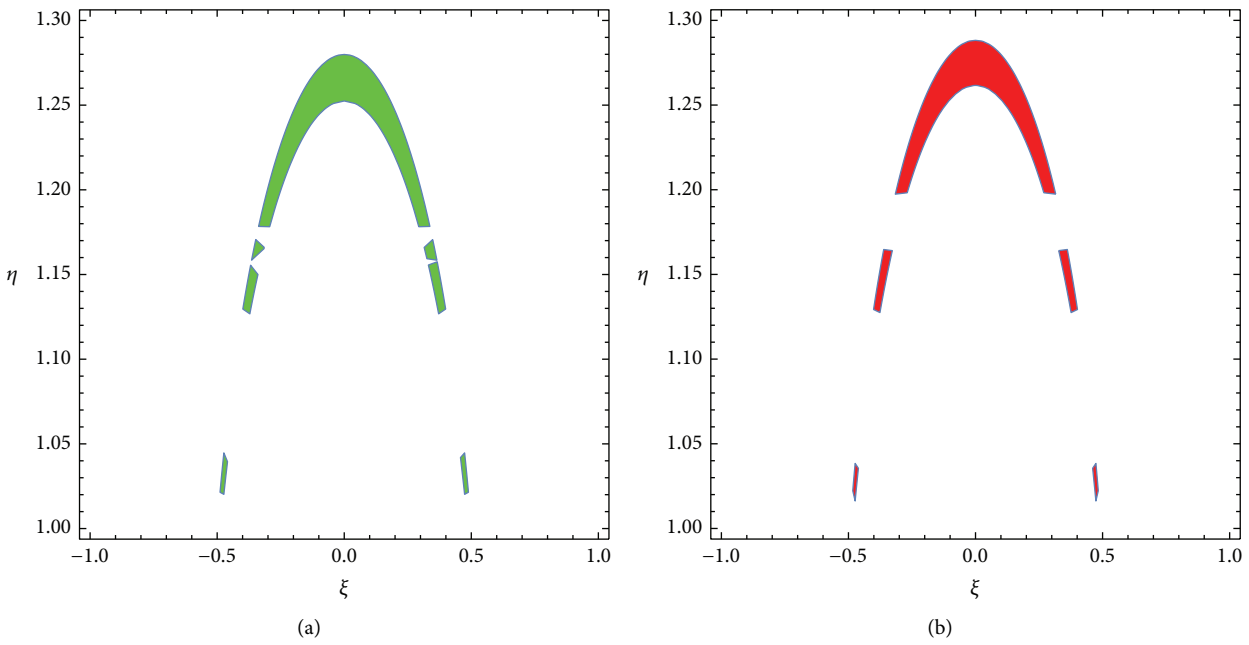

Figure 11: Condition (i): projection of stability regions (a) $b = 0.58$ and $a = 0.68$; (b) $b = 0.60$, and $a = 0.68$.

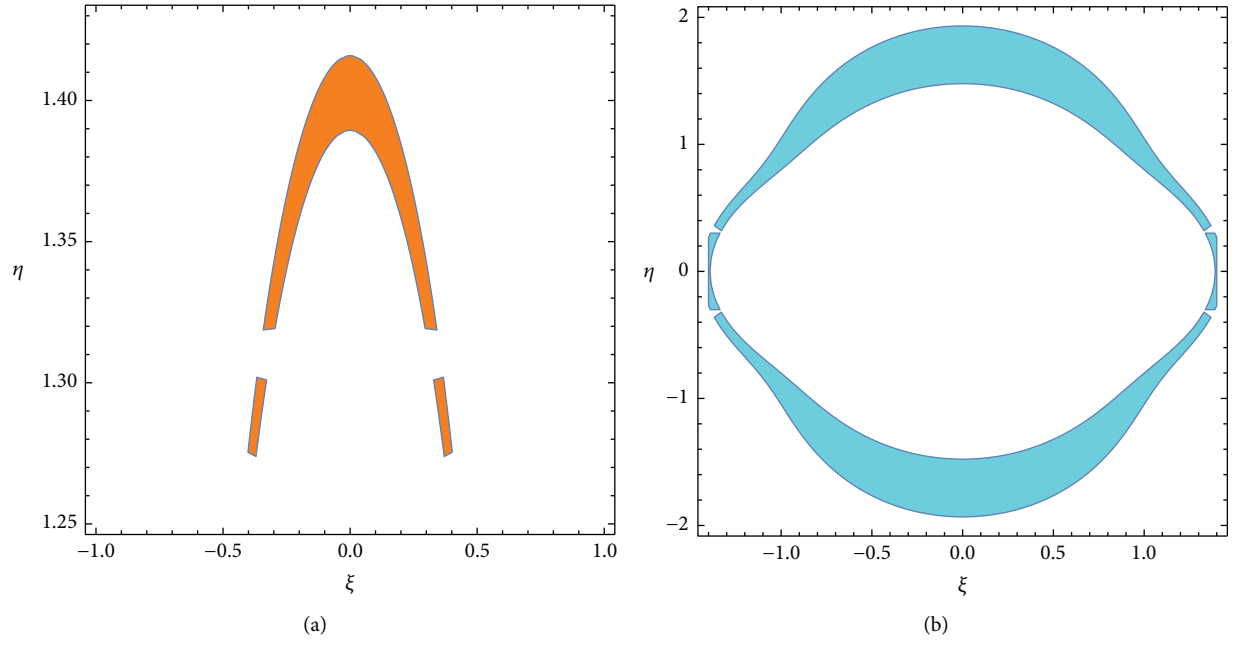

Figure 12: Condition (i): projection of stability regions (a) $b = 0.67$ and $a = 0.78$; (b) $b = 0.80$ and $a = 0.62$.

$$f_1'(\eta) = 1 + \frac{2m_0}{\eta^3} + 2m\left(\frac{3\eta^2}{\left(a^2+\eta^2\right)^{5/2}} - \frac{1}{\left(a^2+\eta^2\right)^{3/2}}\right) + 2\tilde{m}\left(\frac{1}{(b+\eta)^3} + \frac{1}{(\eta-b)^3}\right), \tag{23}$$

$(a^2+\eta^2)^{3/2}$ in equation (23) is the only term that can make the derivative negative for $\eta \in (0, b)$, and as a result, $f_1'(\eta) > 0$, which indicates that the equilibrium points in the interval $(0, b)$ exist and are unique.

5.3. $\eta > b$. When $\eta > b$, equation (21) is rewritten as

$$f_2(\eta) = \eta - \frac{m_0}{\eta^2} - \frac{2m\eta}{\left(a^2+\eta^2\right)^{3/2}} - \tilde{m}\left(\frac{1}{(\eta-b)^2} + \frac{1}{(b+\eta)^2}\right). \tag{24}$$

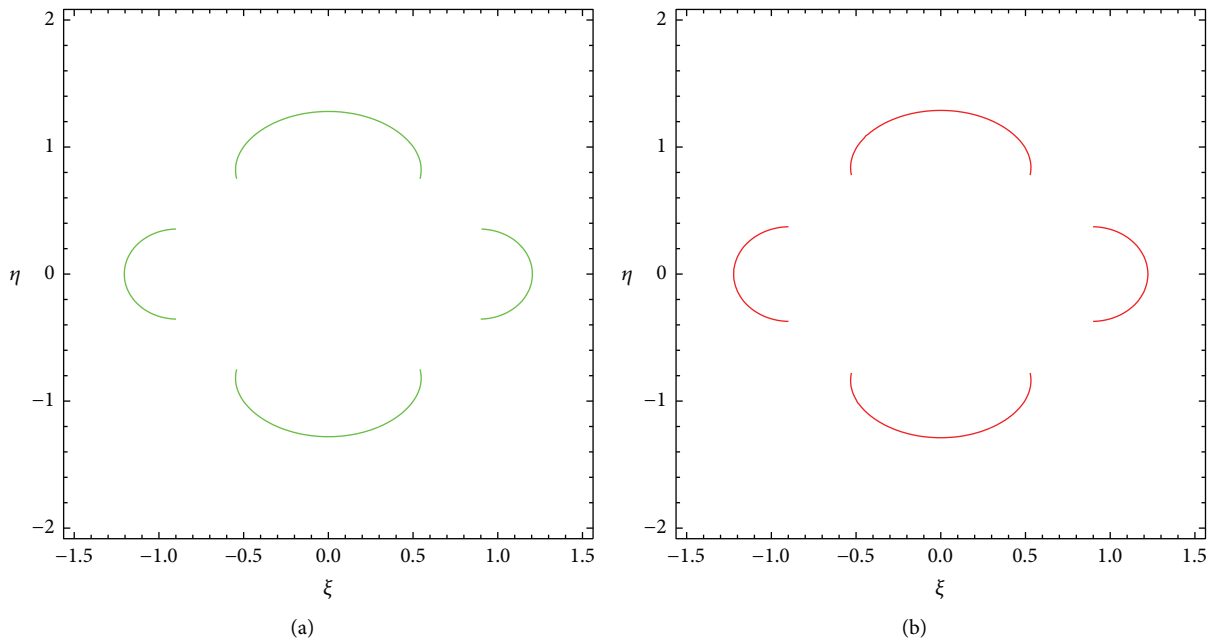

Figure 13: Condition (ii): projection of stability regions (a) $b = 0.58$ and $a = 0.68$; (b) $b = 0.60$ and $a = 0.68$.

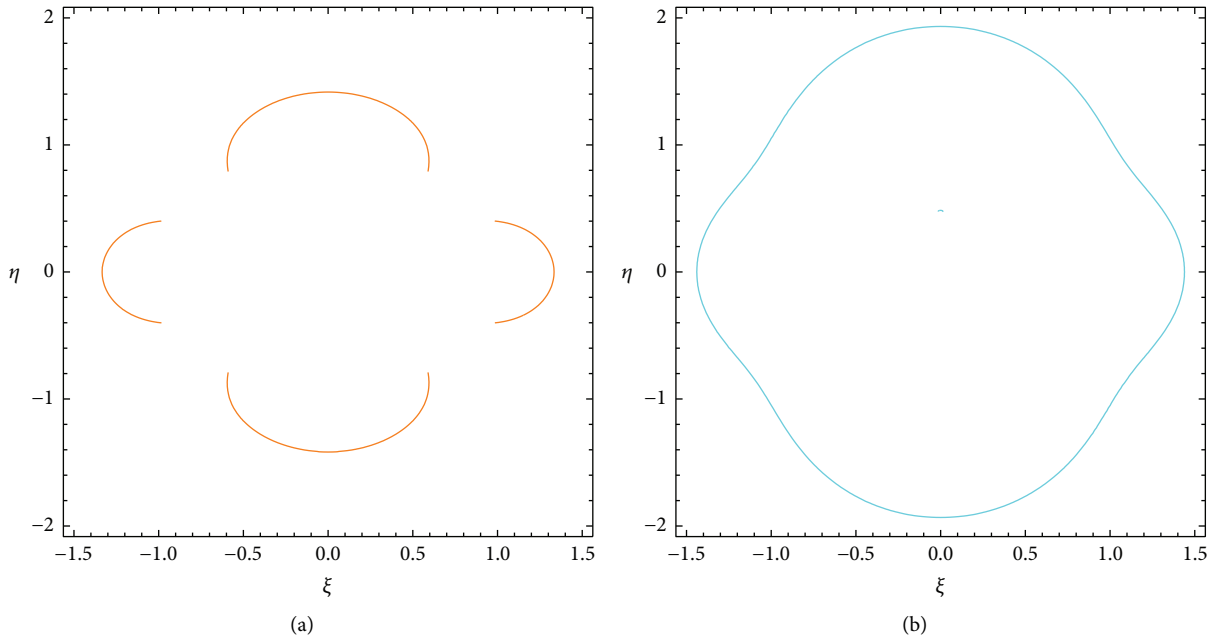

Figure 14: Condition (ii): projection of stability regions (a) $b = 0.67$ and $a = 0.78$; (b) $b = 0.80$ and $a = 0.62$.

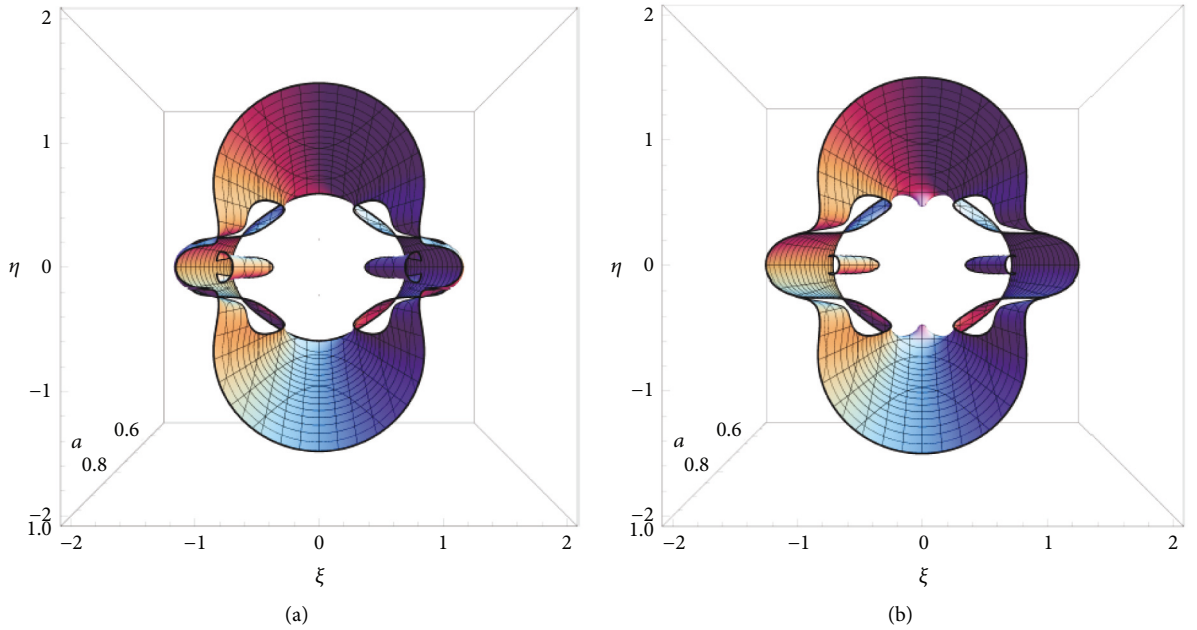

Figure 15: Projection of stability regions (a) $b = 0.58$ and $0.5 < a < 1$; (b) $b = 0.60$ and $0.5 < a < 1$.

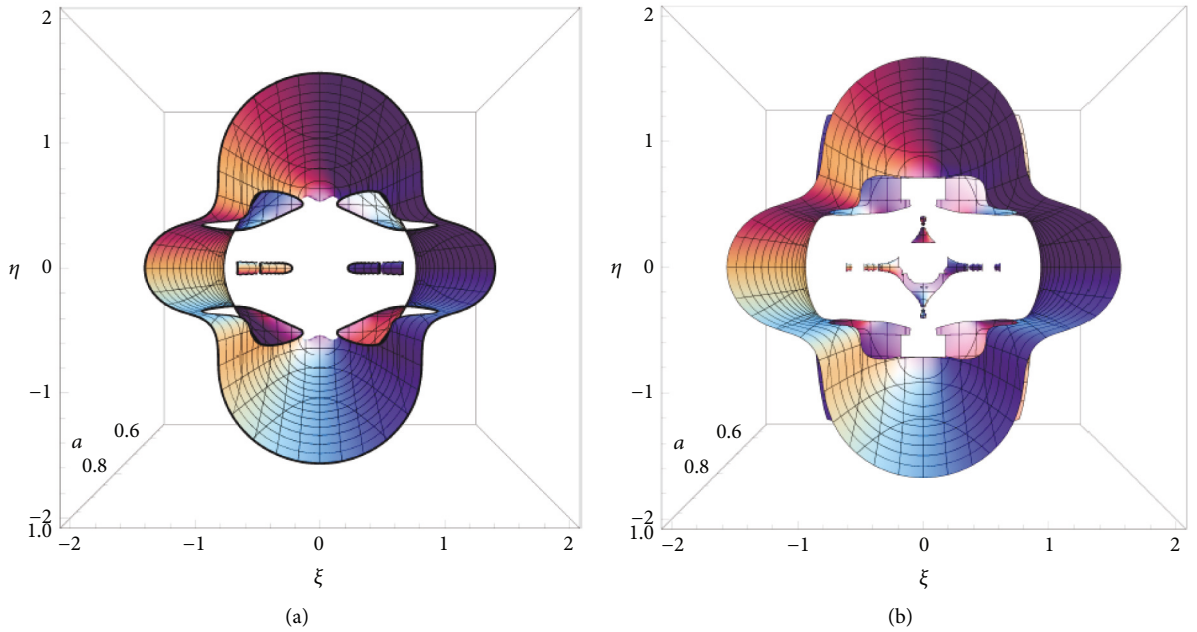

Figure 16: Projection of stability regions (a) $b = 0.67$ and $0.5 < a < 1$; (b) $b = 0.80$ and $0.5 < a < 1$.

For $\eta \in (b, \infty)$ and $b \in (0.5, 1)$, when $\eta \approx b$, $f_2(\eta) < 0$, and when $\eta \approx \infty$, $f_2(\eta) > 0$; thus, the mean value theorem implies that $f_2(\eta)$ has at least one zero when $\eta \in (b, \infty)$. The derivative of equation (24) with respect to η is

$$f_2'(\eta) = 1 + \frac{2m_0}{\eta^3} + 2m\left(\frac{3\eta^2}{\left(a^2+\eta^2\right)^{5/2}} - \frac{1}{\left(a^2+\eta^2\right)^{3/2}}\right) + 2\tilde{m}\left(\frac{1}{(b+\eta)^3} + \frac{1}{(\eta-b)^3}\right). \quad (25)$$

The equilibrium solution's uniqueness for $y > b$ can be easily proved using the same technique as for $0 < y < b$.

Then, there are total 16 equilibrium points for case-I and out of which $L_{5,6,7,8}$ are along η axis, while $L_{1,2,3,4}$ are on ξ axis; similarly for case-II, III, and IV, there are four equilibrium points on each coordinate axis for distinct values of a and b, but the number of equilibrium points is different for other cases, which can be seen from the subfigures (i), (iii), (v), and (vii) of Figure 6.

Table 1: Equilibrium points, eigenvalues, and stability status when $b = 0.58$ and $a = 0.68$.

Equilibrium point	Eigenvalues	Stability
On the coordinate axis		
$L_{1,2} = (\pm 1.183771, 0)$	$\pm 0.067596, \pm 2.670587i$	Unstable
$L_{3,4} = (\pm 0.183968, 0)$	$\pm 7.279086, \pm 10.945510i$	Unstable
$L_{5,6} = (0, \pm 1.158556)$	$\pm 0.500651, \pm 2.791424i$	Unstable
$L_{7,8} = (0, \pm 0.116046)$	$\pm 15.176878, \pm 21.692684i$	Unstable
Off the coordinate axis		
$L_{9,10,11,12} = (0.347976, \pm 0.256131)$	$\pm 1.138065i, \pm 3.593599i$	Stable
$L_{13,14,15,16} = (\pm 0.716623, \pm 0.684335)$	$\mp 0.479573i, \pm 2.668968i$	Stable

Table 2: Equilibrium points, eigenvalues, and stability status when $b = 0.60$ and $a = 0.68$.

Equilibrium point	Eigenvalues	Stability
On the coordinate axis		
$L_{1,2} = (\pm 1.183772, 0)$	$\pm 0.209362, \pm 2.693806i$	Unstable
$L_{3,4} = (\pm 0.228309, 0)$	$\pm 5.091753, \pm 8.027477i$	Unstable
$L_{9,10} = (0, \pm 1.169283)$	$\pm 0.500956, \pm 2.792577i$	Unstable
$L_{11,12} = (0, \pm 0.164938)$	$\pm 8.849253, \pm 12.907057i$	Unstable
Off the coordinate axis		
$L_{5,6,7,8} = (0.228064, \pm 0.058906)$	$\pm 4.765442, \pm 7.656460i$	Unstable
$L_{13,14,15,16} = (\pm 0.334768, \pm 0.250108)$	$\mp 1.088025i, \pm 3.645851i$	Stable
$L_{17,18,19,20} = (\pm 0.716623, \pm 0.684335)$	$\mp 0.508226i, \pm 2.666074i$	Stable

Table 3: Equilibrium points, eigenvalues, and stability status when $b = 0.67$ and $a = 0.78$.

Equilibrium point	Eigenvalues	Stability
On the coordinate axis		
$L_{1,2} = (\pm 1.147893, 0)$	$\pm 1.125396, \pm 3.220510i$	Unstable
$L_{3,4} = (\pm 0.465536, 0)$	$\pm 1.381845, \pm 3.742671i$	Unstable
$L_{5,6} = (0, \pm 1.245704)$	$\pm 0.715462, \pm 2.911764i$	Unstable
$L_{7,8} = (0, \pm 0.287148)$	$\pm 2.273632, \pm 4.422842i$	Unstable
Off the coordinate axis		
$L_{9,10,11,12} = (\pm 0.782825, \pm 0.505983)$	$\mp 0.673476i, \pm 2.735112i$	Stable

Table 4: Equilibrium points, eigenvalues, and stability status when $b = 0.80$ and $a = 0.62$.

Equilibrium point	Eigenvalues	Stability
On the coordinate axis		
$L_{1,2} = (\pm 1.239106, 0)$	$\pm 0.646502, \pm 2.834110i$	Unstable
$L_{3,4} = (\pm 0.230153, 0)$	$\pm 9.177227, \pm 13.194850i$	Unstable
$L_{5,6} = (0, \pm 1.108360)$	$\pm 3.715368, \pm 3.365771i$	Unstable
$L_{7,8} = (0, \pm 0.519657)$	$\pm 2.864727, \pm 3.088526i$	Unstable
Off the coordinate axis		
$L_{9,10,11,12} = (\pm 0.421763, \pm 0.819726)$	$\mp 2.317673, \pm 3.0801580i$	Unstable

5.4. Equilibrium Solutions: Off the Coordinate Axes. The mass parameters a and b, which we have numerically confirmed, determine the number and location of the equilibrium points, which is illustrated in subfigures (i), (iii), (v), and (vii) of Figure 6. For case-I, there are eight off-coordinate axis equilibrium points; for case-II, there are 12 off-coordinate axis equilibrium points, the majority of which are clustered around the central mass m_0. Cases III and IV contain 4 equilibrium points that cluster around m and $\tilde{m}$ off the coordinate axis.

6. Stability Analysis

We represent the location of an equilibrium point in our problem by the coordinates (ξ, η) and consider a small displacement from the equilibrium point to be (ξ_0, η_0) in order to linearize around the equilibrium point, and then, the new location of the equilibrium points will be $(\xi + \xi_0, \eta + \eta_0)$. The system in equations (14) is subjected to Taylor series expansion, yielding the following set of linearized equations:

$$\ddot{\xi}_0 - 2\dot{\eta}_0 = \xi_0\Omega_{\xi\xi} + \eta_0\Omega_{\xi\eta},$$
$$\ddot{\eta}_0 + 2\dot{\xi}_0 = \xi_0\Omega_{\xi\eta} + \eta_0\Omega_{\eta\eta}. \tag{26}$$

The linearized equations in the matrix form is

$$\begin{pmatrix} \dot{\xi}_0 \\ \dot{\eta}_0 \\ \ddot{\xi}_0 \\ \ddot{\eta}_0 \end{pmatrix} = \begin{pmatrix} 0 & 0 & 1 & 0 \\ 0 & 0 & 0 & 1 \\ \Omega_{\xi\xi} & \Omega_{\xi\eta} & 0 & 2 \\ \Omega_{\xi\eta} & \Omega_{\eta\eta} & -2 & 0 \end{pmatrix} \begin{pmatrix} \xi_0 \\ \eta_0 \\ \dot{\xi}_0 \\ \dot{\eta}_0 \end{pmatrix}. \tag{27}$$

Let

$$\Upsilon = \begin{pmatrix} \xi_0 \\ \eta_0 \\ \dot{\xi}_0 \\ \dot{\eta}_0 \end{pmatrix} \text{ and } \mathscr{M} = \begin{pmatrix} 0 & 0 & 1 & 0 \\ 0 & 0 & 0 & 1 \\ \Omega_{\xi\xi} & \Omega_{\xi\eta} & 0 & 2 \\ \Omega_{\xi\eta} & \Omega_{\eta\eta} & -2 & 0 \end{pmatrix}. \tag{28}$$

The equation in (27) can be written as

$$\dot{\Upsilon} = \mathscr{M}\Upsilon. \tag{29}$$

From $\mathscr{M}$, we have

$$\Psi^4 + \alpha\Psi^2 + \beta = 0, \tag{30}$$

where $\alpha = 4 - \Omega_{\xi\xi} - \Omega_{\eta\eta}$ and $\beta = \Omega_{\xi\xi}\Omega_{\eta\eta} - \Omega_{\xi\eta}^2$.

Let $\Psi^2 = \lambda$, then equation (30) reduces to

$$\lambda^2 + \alpha\lambda + \beta = 0. \tag{31}$$

For an equilibrium point to be linearly stable under a slight disturbance, all four roots of equation (30) must be completely imaginary. As a result, the two roots of equation (31)

$$\lambda_{\pm} = \frac{-\alpha \pm \sqrt{\alpha^2 - 4\beta}}{2}, \tag{32}$$

must be real and negative. For $\lambda_{\pm} < 0$, we must have

$$(i)\alpha > 0 \text{ and } 0 < \beta \leq \alpha^2/4,$$
$$\text{or } (ii)\alpha > 0 \text{ and } \alpha^2 - 4\beta = 0. \tag{33}$$

The regions of stability when either condition (i) or (ii) holds true have been determined and presented in Figures 11–14. The stability areas corresponding to the four cases for different values of a and b are shown in Figures 15 and 16, where b is fixed at 0.58, 0.60, 0.67, and 0.80, and the regions are projected across the whole domain of the mass parameter a, that is, $0.5 < a < 1$. We investigated the stability of the equilibrium points found in the preceding section for each of the four different cases, and many off-coordinate stable equilibrium points were discovered; the results are reported in Tables 1–4.

7. Conclusion

Mass parameters a and b are used to examine the restricted rhomboidal six-body problem in depth. A point mass, m_0, is put at the intersection of two diagonals of the rhombus, and the remaining four point masses are arranged in such a way that they preserve a rhomboidal central configuration during their two-by-two motion. The point masses at the opposite vertices of a rhombus are supposed to be the same, that is, $m_1 = m_2 = m$ and $m_3 = m_4 = \tilde{m}$. In a synodical coordinate system, the motion of the sixth test mass, m_5, which has an infinitesimal mass relative to the other five masses, that is, $(m_5 \ll m_{0,1,2,3,4})$, is investigated for both the equilibrium points and their linear stability. A significant shift in the position and number of equilibrium points was found in four cases with the variations of mass parameters a and b. Cases-I to IV have 16, 20, 12, and 12 equilibrium points respectively, with case-I and case-II having eight off-the-coordinate-axis stable equilibrium points, case-III having four off-the-coordinate-axis stable equilibrium points, and case-IV having no on or off-the-coordinate-axis stable equilibrium points. The regions for the possible motion of m_5 have been discovered, and it has been observed that as the Jacobian constant C increases, the permissible region of motion expands, and the values of C for which the regions of the possible motion become disconnected or partially disconnected have also been discovered. We also have numerically verified the stability regions for different cases, which shows the presence of stable equilibrium points.

Data Availability

No data were used for the article.

Conflicts of Interest

The authors declare that there are no conflicts of interest regarding the publication of this article.

References

[1] L. Euler, "On the role and the prooperties of n-body central configuration," *Celestial Mechanics*, vol. 21, no. 1, pp. 9–20, 1980.

[2] Z. Xia, "On the role and the properties of n-body central configuration," *Celestial Mechanics*, vol. 91, no. 1, pp. 168–179, 1991.

[3] J. Llibre and L. F. Mello, "New central configurations for the planar 7-body problem," *Nonlinear Analysis: Real World Applications*, vol. 10, no. 4, pp. 2246–2255, 2009.

[4] Y. Deng, B. Li, and S. Zhang, "Four-body central configurations with adjacent equal masses," *Journal of Geometry and Physics*, vol. 114, pp. 329–335, 2017.

[5] M. Marchesin, "Stability of a rhomboidal configuration with a central body," *Astrophysics and Space Science*, vol. 362, no. 1, 2017.

[6] D. G. Saari, "On the role and the properties of n body central configurations," *Celestial Mechanics*, vol. 21, no. 1, pp. 9–20, 1980.

[7] R. Moeckel, "On central configurations," *Mathematische Zeitschrift*, vol. 205, no. 1, pp. 499–517, 1990.

[8] J. Casasayas, J. Llibre, and A. Nunes, "Central configurations of the planar 1 + n body problem," *Celestial Mechanics and Dynamical Astronomy*, vol. 60, no. 2, pp. 273–288, 1994.

[9] Y. Long and S. Sun, "Collinear central configurations and singular surfaces in the mass space," *Archive for Rational Mechanics and Analysis*, vol. 173, no. 2, pp. 151–167, 2004.
[10] Z. Xia, "Convex central configurations for the n-body problem," *Journal of Differential Equations*, vol. 200, no. 2, pp. 185–190, 2004.
[11] M. Hampton, "Stacked central configurations: new examples in the planar five-body problem," *Nonlinearity*, vol. 18, no. 5, pp. 2299–2304, 2005.
[12] M. Hampton and M. Santoprete, "Seven-body central configurations: a family of central configurations in the spatial seven-body problem," *Celestial Mechanics and Dynamical Astronomy*, vol. 99, no. 4, pp. 293–305, 2007.
[13] J. Llibre and L. F. Mello, "New central configurations for the planar 5-body problem," *Celestial Mechanics and Dynamical Astronomy*, vol. 100, no. 2, pp. 141–149, 2008.
[14] Z. Xie, "Super central configurations of the n-body problem," *Journal of Mathematical Physics*, vol. 51, no. 4, Article ID 042902, 2010.
[15] J. Shi and Z. Xie, "Classification of four-body central configurations with three equal masses," *Journal of Mathematical Analysis and Applications*, vol. 363, no. 2, pp. 512–524, 2010.
[16] M. S. Suraj, E. I. Abouelmagd, R. Aggarwal, and A. Mittal, "The analysis of restricted five–body problem within frame of variable mass," *New Astronomy*, vol. 70, no. 1, pp. 12–21, 2019.
[17] E. E. Zotos and K. Papadakis, "Orbit classification and networks of periodic orbits in the planar circular restricted five-body problem," *International Journal of Non-linear Mechanics*, vol. 111, pp. 119–141, 2019, accepted manuscript.
[18] J. L. Cornelio, M. Alvarez-Ramírez, and J. M. Cors, "Central configurations in the five-body problem: rhombus plus one," *Qualitative theory of dynamical systems*, vol. 20, no. 2, pp. 51–13, 2021.
[19] C. Wilson, "Clairaut's calculation of the eighteenth-century return of Halley's comet," *Journal for the History of Astronomy*, vol. 24, no. 1-2, pp. 1–15, 1993.
[20] J.-P. Luminet, *Clairaut, Alexis-Claude*, , pp. 431-432, Biographical Encyclopedia of Astronomers, 2014.
[21] A. Ollongren, "On a particular restricted five-body problem an analysis with computer algebra," *Journal of Symbolic Computation*, vol. 6, no. 1, pp. 117–126, 1988.
[22] K. E. Papadakis and S. S. Kanavos, "Numerical exploration of the photogravitational restricted five-body problem," *Astrophysics and Space Science*, vol. 310, no. 1-2, pp. 119–130, 2007.
[23] M. Marchesin and C. Vidal, "Stability in a rhomboidal 5-body problem with generalized central forces," *Journal of Mathematical Physics*, vol. 54, no. 10, p. 102902, 2013.
[24] R. Aggarwal, A. Mittal, M. S. Suraj, and V. Bisht, "The effect of small perturbations in the coriolis and centrifugal forces on the existence of libration points in the restricted four-body problem with variable mass," *Astronomische Nachrichten*, vol. 339, no. 6, pp. 492–512, 2018.
[25] L. F. Mello, F. E. Chaves, A. C. Fernandes, and B. A. Garcia, "Stacked central configurations for the spatial six-body problem," *Journal of Geometry and Physics*, vol. 59, no. 9, pp. 1216–1226, 2009.
[26] M. J. Idrisi and M. S. Ullah, "Central-body square configuration of restricted six-body problem," *New Astronomy*, vol. 79, Article ID 101381, 2020.
[27] A. A. Ansari, K. Meena, and S. N. Prasad, "Perturbed six-body configuration with variable mass," *Romanian Astronomical Journal*, vol. 30, no. 2, pp. 135–152, 2020.
[28] M. Kulesza, M. Marchesin, and C. Vidal, "Restricted rhomboidal five-body problem," *Journal of Physics A: Mathematical and Theoretical*, vol. 44, no. 48, Article ID 485204, 2011.
[29] M. Marchesin and C. Vidal, "Spatial restricted rhomboidal five-body problem and horizontal stability of its periodic solutions," *Celestial Mechanics and Dynamical Astronomy*, vol. 115, no. 3, pp. 261–279, 2013.
[30] M. A. R. Siddique, A. R. Kashif, M. Shoaib, and S. Hussain, "Stability analysis of the rhomboidal restricted six-body problem," *Advances in Astronomy*, vol. 2021, Article ID 5575826, 2115 pages, 2021.
[31] M. S. Suraj, S. S. Alhowaity, and R. Aggarwal, *Fractal Basins of Convergence in the Restricted Rhomboidal Six-Body Problem*, New Astronomy, Article ID 101798, 2022.
[32] R. Broucke, "Periodic orbits in the restricted three body problem with earth-moon masses," Technical Reports Series, National Aeronautics and Space Administration, Washington, DC, USA, 1968.